AGU PUBLICATIONS

JGR

Journal of Geophysical Research: Space Physics

RESEARCH ARTICLE
10.1002/2013JA019582

Key Points:
- 3D ionospheric tomography
- GPS TEC data from GEONET
- 3D tomography and simulation using NeQuick model

Correspondence to:
G. K. Seemala,
gopi.seemala@gmail.com

Citation:
Seemala, G. K., M. Yamamoto, A. Saito, and C.-H. Chen (2014), Three-dimensional GPS ionospheric tomography over Japan using constrained least squares, *J. Geophys. Res. Space Physics*, *119*, doi:10.1002/2013JA019582.

Received 30 OCT 2013
Accepted 28 FEB 2014
Accepted article online 4 MAR 2014

Three-dimensional GPS ionospheric tomography over Japan using constrained least squares

Gopi K. Seemala[1,2], Mamoru Yamamoto[1], Akinori Saito[3], and Chia-Hung Chen[4]

[1]Research Institute for Sustainable Humanosphere, Kyoto University, Kyoto, Japan, [2]Indian Institute of Geomagnetism, Mumbai, India, [3]Department of Geophysics, Kyoto University, Kyoto, Japan, [4]Department of Earth Science, National Cheng Kung University, Tainan, Taiwan

Abstract A new three-dimensional GPS ionospheric tomography technique is developed that uses total electron content (TEC) data from the dense Global Position System (GPS) receiver network, GPS Earth Observation Network (GEONET) in Japan, and it will not require an ionospheric model as the initial guess that will bias the reconstruction of electron density. The GEONET is operated by Geospatial Information Authority of Japan and consists of more than 1200 receivers; this high density and wide coverage helps to reconstruct the electron density distribution in the ionosphere with high spatial resolution. This tomography technique uses a constrained least squares fit to reconstruct the three-dimensional electron density distributions. This method is different to most other techniques as they require a background ionospheric model as an initial guess that could bias the reconstructed electron density. It rather uses a prior condition that the electron density should not exceed a certain value that is determined by the restrain parameter, which is derived from the NeQuick model. Its independency of the initial guess from a model will make it useful even in disturbed conditions. This paper presents results that are obtained by using this new tomographic technique. The reconstruction of three-dimensional ionospheric tomograms is demonstrated using the GPS data, and the reliability and robustness are checked with simulated tomograms obtained using the synthetic GPS-TEC data produced using NeQuick model.

1. Introduction

In the recent years, ionospheric total electron content (TEC) measurements have regained importance as there was an exponential usage and growth of satellite-based navigation applications in various fields, like Global Positioning System (GPS). The radio signal delay caused by the ionospheric electron content and irregularities are among the major factors affecting the transionospheric navigation and communication systems. Also, the TEC measurements and models are important for applications such as error correction to operational systems, satellite navigation and orbit determination, satellite altimetry, determining the scintillation of radio wave, etc. Thus, deriving and studying the three-dimensional distribution of ionospheric electron density is very useful to study the ionospheric phenomena that effect the radio wave propagation.

Austen et al. [1988] suggested two-dimensional tomographic technique using the TEC data from beacons from low-Earth orbit, which applies medical tomography to study the ionosphere. But the ionospheric observations were limited by the minimum elevation angle, rate of data collected, and the number and spacing of receivers in the array. And also, the tomography technique requires the knowledge of number density and is also insensitive to stratified ionosphere [*Yeh and Raymund*, 1991]. Hence, a prior data have to be included from other sources; the reconstructed number density is only accurate up to the class of background ionosphere. *Austen et al.* [1986, 1988] used the line-of-sight TEC data from naval navigational satellite system, flying around 1100 km altitude, to reconstruct the two-dimensional structure of the ionospheric electron density. Later, many studies were done on ionospheric tomography [see *Austen et al.*, 1988; *Raymund et al.*, 1990, 1994; *Raymund*, 1995; *Fremouw et al.*, 1992; *Andreeva et al.*, 1992; *Kersley et al.*, 1993; *Hansen et al.*, 1997; *Howe et al.*, 1998], and most investigators used the total electron content (TEC) measurements collected by a chain of meridionally aligned stations all simultaneously observing a rapidly orbiting radio beacon. Most of these tomography methods reconstruct the two-dimensional electron density along the satellite-to-receiver flying plane and their accuracy being limited by the background ionospheric model used in addition to the incomplete ray geometry, background, and measurement noise. Therefore, radio tomography is more ill-posed compared to the widely known computer tomography in medical applications [*Zhai and Cummer*, 2005].

The GPS has more than 24 satellites around 20,200 km altitude in six orbital planes whose inclination angle is 55°, which can provide the global coverage of observations. The TEC value along the raypath between the GPS satellite and GPS receivers can be measured by the dual-frequency ($f_1 = 1.57542$ GHz and $f_2 = 1.22760$ GHz) GPS signals continuously. Measurement of TEC by using the GPS receivers is now widely used; these TEC measurements will be also referred as GPS-TEC. As there are always several GPS satellites available for the measurement, it is a very good tool for constant monitoring of the ionosphere. One of the most dense and wide network of the GPS network is GEONET operated by Geospatial Information Authority of Japan (GSI). This is a network of more than 1200 GPS receivers over the whole Japan with averaged spatial resolution of 25 km. The GPS-TEC from the GEONET of 30 s is used for studies of ionospheric disturbances [*Saito et al.*, 1998, 2001]. By taking the advantage of this dense GPS network, a good spatial and temporal resolution of TEC distribution can be obtained.

At Kyoto University, we have developed a new three-dimensional GPS ionospheric tomography technique that uses GPS-TEC from the dense GPS network of GEONET. This technique does not require an ionospheric model as initial guess; the algorithm uses constrained least squares fit to derive electron density distribution even in disturbed conditions [*Fehmers et al.*, 1998]. This method is different to most ionospheric tomographic techniques [*Ma et al.*, 2005; *Fridman et al.*, 2006] as they require a background ionospheric model as an initial guess that could bias the resulting electron density tomogram. *Fridman et al.* [2006] used International Reference Ionosphere 2000 as the initial background electron density for 3-D reconstruction from GPS-TEC data; the solution was inclined to the background model when enough data were not present. And *Ma et al.* [2005] used Neural Network to reconstruct 3-D electron density using GPS-TEC and ionosonde data; ionosonde data were very effective in improving the vertical density distribution as it directly provides vertical profile.

This technique rather uses a prior condition that the electron density should not exceed a certain value that is determined by the restrain parameter and with an assumption that the gradient of the election density is not large in the horizontal plane and can be large in the vicinity of the F_2 peak. The algorithm is designed to be independent of any ionospheric and plasmaspheric density models for the initial condition. Because the three-dimensional ionospheric tomography describes the characteristics of the entire ionosphere, rather than only in one plane (unlike two-dimensional tomography), it is expected that 3-D electron density profiling of the ionosphere has an enhancement in terms of understanding various phenomenon in the ionosphere.

This paper discusses and presents the results of this new three-dimensional GPS ionospheric tomography algorithm. The electron density images that are produced using the new tomography technique using the GPS-TEC data from Japan's GEONET are evaluated using simulated tomograms obtained using the simulated GPS-TEC data produced using NeQuick model [*Radicella and Leitinger*, 2001].

2. Data and Methodology

The Geographical Survey Institute (GSI) of Japan has launched its nationwide GPS array project in April 1994 and has installed more than 1200 receivers in Japan, called GPS Earth Observation Network (GEONET) [*Miyazaki et al.*, 1997; *Tsuji et al.*, 1995; *Iwabuchi et al.*, 1997]. The average spatial resolution of installed GPS receivers is approximately 25 km. Each GPS receiver measures signals simultaneously from typically six to seven satellites, and the GPS data are sampled every 30 s. By taking advantage of this dense network, we can have TEC data with a very high spatial resolution and time resolution. In the calculation of absolute TEC, a least squares fitting procedure is used to remove instrumental biases inherent in the GPS satellite and receiver [*Otsuka et al.*, 2002]. An elevation mask angle of 20° is set for the GPS-TEC data used in this present study.

The initial step in the tomography process is to obtain integral measurements of the ionosphere, ideally along many paths at many different viewing angles, which is satisfied to an extent with the advantage of having GPS data from GEONET. In order to have a uniform density of GPS data with maximum coverage over Japan, we have chosen station locations such that a single GPS station is selected in each $0.25° \times 0.25°$ latitude and longitude grid for the analysis. Figure 1 shows distribution of 751 GPS receiver stations that were chosen so that there is only one station in each $0.25° \times 0.25°$ grid. TEC data from these stations are used for the GPS tomography on 23 May 2012 in the following section. It can be clearly seen that there is good and almost uniform spatial coverage of GPS stations over Japan, which is an advantage for ionospheric tomography in this region.

This new GPS tomography technique to reconstruct the ionospheric three-dimensional electron density structure was developed with the constrained least squares method without depending on the ionospheric

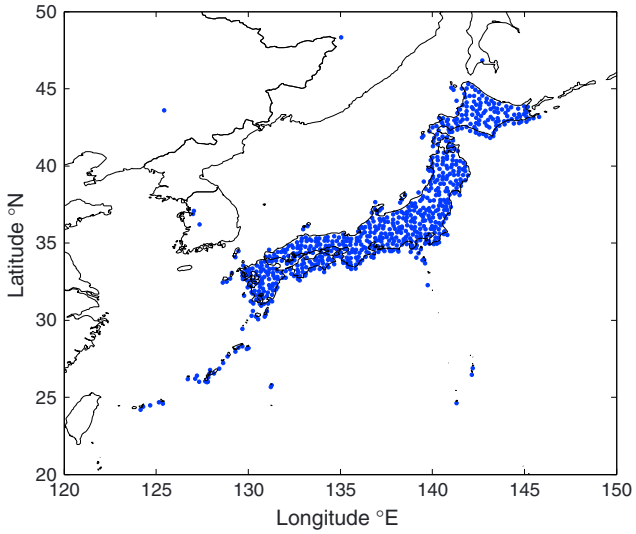

Figure 1. Locations of selected GPS receiver station locations (indicated by blue dots) from GEONET data.

background model as the initial guess. But rather, this technique uses a prior condition that sets the wider boundary conditions for the resultant electron density profile so that the algorithm has enough flexibility to produce electron densities that can be similar to the ambient electron density in the ionosphere. In the present study, this algorithm needs data from single epoch to compute the three-dimensional tomograms. This flexibility, and independent on the background ionospheric model, makes the algorithm suitable to be used to derive the three-dimensional electron density tomograms even in the disturbed conditions.

As shown in schematic in Figure 2, the three-dimensional space with the altitude from 80 km to 20,200 km, around the height of GPS satellite, was divided into three-dimensional pixels or voxels. The resolution and the range set for the GPS tomography are as follows. The horizontal resolution is set to 1°, in which the latitudinal range is from 20° to 50°N and the longitudinal range is from 120° to 150°E. The vertical range is from 80 km to 20,000 km altitude, which has a mixed resolution of 20 km from 80 to 600 km range, 50 km resolution from 600 to 900 km range, 100 km resolution from 1000 to 2000 km, and 5000 km resolution from there onward to 20000 km.

The GPS-TEC observation data along a raypath "*i*" from a GPS satellite to a GPS receiver can be written as

$$\sum_j A_{ij} x_j = b_i \tag{1}$$

where A_{ij} is a $m \times n$ matrix which indicates the length of path i in each of the voxel j, $i = 1,\ldots,m$ and $j = 1,\ldots,n$. The number of voxels is "n", x_j indicates the electron density in voxel j, and b_i is the TEC value along one GPS observational path i. The simplest way to calculate the electron density, the "x matrix", is just using the least squares method. However, due to the lack of horizontal GPS observation paths and the numerous unpassed grids, "A" matrix is a sparse matrix and the solutions cannot be found by a straightforward solution of least squares method. In order to solve the equation (1), the least squares fitting with a constrained condition was used. The cost function, $J(x)$, with constrained least squares fitting used in this study was defined as

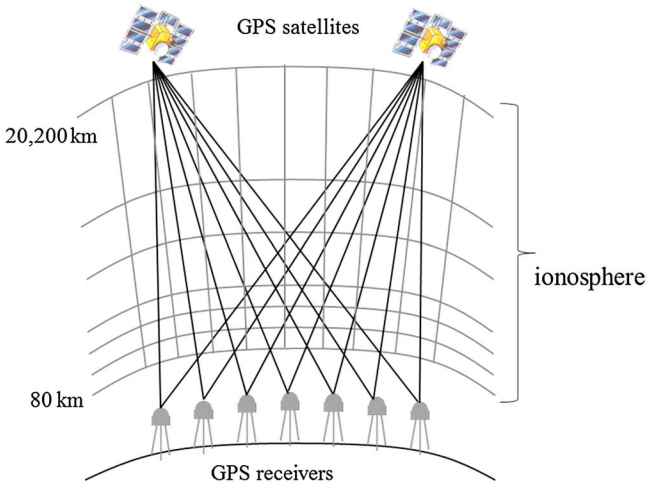

Figure 2. Schematic showing grid division of ionospheric region from 80 km to 20,200 km altitude and observation paths between GPS receivers and GPS satellite [*Chen*, 2012].

$$J(x) = \|b - Ax\|^2 + \lambda \|Wx\|^2 \tag{2}$$

where

$$Wx = \sum_{j=1}^{n} \sum_{k=1}^{6} C_{jk}\left(x_j - x_{jk}\right) \tag{3}$$

The first term in the right of equation (2) is the normal least squares fit and the second term is the constrain condition. Where W is the weight matrix containing the restrain parameter that varies with altitude and latitude. The weight term is selected as summation

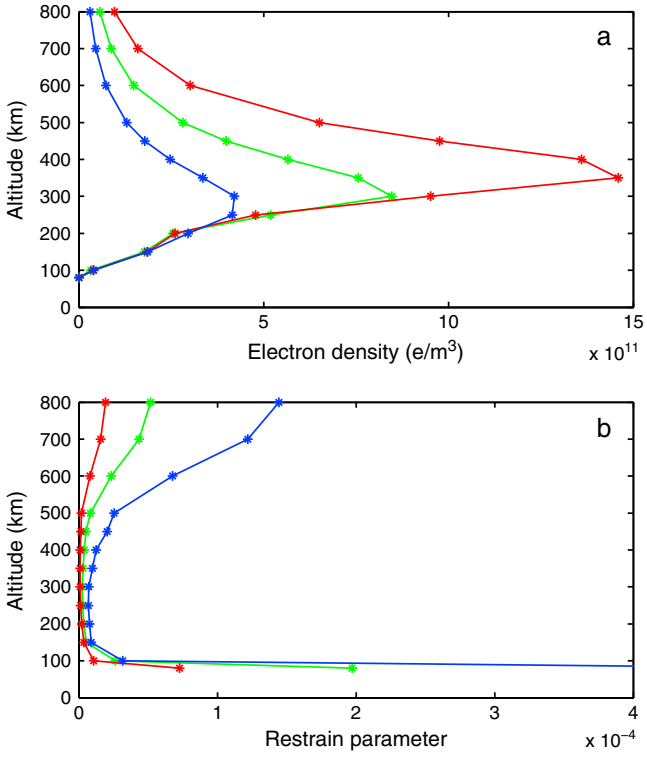

Figure 3. (a) Electron density profiles from NeQuick model at 20, 35, and 50°N latitudes indicated with colors red, blue, and green, respectively, at 135°E longitude at time 03:30 UT on 23 May 2012 and (b) the derived restrain parameter for the density profiles indicated by respective colors.

of density differences with six neighboring voxels "x_{jk}" around each grid point or a voxel "x_j" as given in equation (3). The value C_{jk}, called as restrain parameter, indicates the weighting of the constrained condition. In the constrained condition it is assumed that the spatial gradient of the election density is relatively smaller than vertical gradient in the tomography space. Therefore, in this study, we set "C_{jk}" that it varies with altitude (80 to 25,000 km) and latitude (20° to 50°N) along the meridian of 135°E. And the value λ, called as hyper parameter, will balance the importance of the two terms in equation (2).

The success of this algorithm is mostly dependent on the selection of the C_{jk} values. This restrain parameter C_{jk} is dynamically derived from the NeQuick model for the time of given GPS data input. Since the electron density varies a lot around the *F* region, a weak restrain parameter is applied from 150 km to 600 km to allow enough room for the electron density to change independent of the model-derived restrain parameter. This tomography technique uses the two-dimensional restrain condition that changes with altitude as well as latitude; rather, it is discrete as only three latitudes that are 15° apart were taken into account to cover the latitude extent of 20° to 50°N region along the meridian of 135°E is used in this tomography. Even though, the restrain parameter is derived from the NeQuick ionospheric model, this resultant restrain parameter is very loosely connected to the model as can be seen in Figure 3. Figure 3 shows the typical derivation of the restrain condition or the prior condition used in the technique. In this technique, the restrain parameter C_{jk} is scaled from the NeQuick-derived electron density profile values by ad hoc coefficients so that the resultant values lie in between 0 and 1. The higher value of restrain parameter (closer to 1) indicates more constraint, and the minimum value (closer to 0) indicates less constraint that leaves room for the resulting electron density to vary more. To compute the restrain parameter, the electron density values derived from NeQuick model are normalized with respect to the maximum value in the profile. These normalized values are subtracted from 1 so that the (complemented) values will become maximum when the electron density is minimum. These values are scaled with ad hoc coefficients that vary with altitude in such a way that the resulting restrain parameter is moderate and shallow around *F* region to have enough room for electron density variations. Figure 3a shows the NeQuick model-derived electron density profiles at latitudes 20°, 35°, and 50°N along longitude 135°E, indicated by colors red, green, and blue respectively at time 03:30 UT on 23 May 2012. Figure 3b shows the derived restrain parameter corresponding to each latitudes indicated by the color code corresponding to Figure 3a. Table 1 shows the ad hoc coefficients for each altitude that are used in deriving the restrain parameter which is shown in Figure 3b for latitudes 20°, 35°, and 50°N, respectively. Figures 3a and 3b are on linear scale, and it can be seen that the restrain parameter independent of the electron density profile is very relaxed from 150 km to 600 km (the lower value indicates weak constraint) that allows the resultant density to change irrespective of the indirect model input used here for restrain parameter.

The hyper parameter "λ" in equation (2), which is another important variable, indicates the weighting of the constraint condition in comparison with the least squares term. The change in hyper parameter changes the

Table 1. Ad Hoc Coefficients Used in Restrain Parameter

Altitude (km s)	Coefficients for 20°N	Coefficients for 35°N	Coefficients for 50°N
80	2.033E-04	5.338E-04	1.497E-03
100	8.338E-05	2.210E-04	3.597E-04
150	5.089E-05	9.396E-05	3.005E-04
200	3.442E-05	8.223E-05	6.040E-04
250	3.334E-05	1.651E-04	1.525E-02
300	7.176E-05	2.625E-06	7.350E-06
350	9.975E-07	7.542E-04	1.162E-03
400	4.510E-04	2.747E-04	6.341E-04
450	1.061E-04	1.879E-04	6.393E-04
500	6.952E-05	2.122E-04	5.800E-04
600	1.437E-04	3.723E-04	1.039E-03
700	1.995E-04	5.250E-04	1.470E-03
800	1.995E-04	5.250E-04	1.470E-03
1,000	2.660E-04	7.000E-04	1.960E-03
2,000	5.225E-04	1.375E-03	3.850E-03
25,000	8.793E-03	2.316E-02	6.489E-02

significance of the constrain condition in the cost function. The large value of hyper parameter indicates that more importance is given for the restrain parameter in the cost function (a strong constraint), and the small value of hyper parameter indicates that the least squares term in the cost function is important for the minimization (weak constraint). It should be noted that these two terms in the right side of equation (2) cannot be simultaneously minima. So it is important to find an optimized value of hyper parameter. In this technique, instead of finding an optimum hyper parameter and then solve the cost function (equation (2)), the cost function is solved with different values of hyper parameter. Among those different solutions available, the best solution is chosen when both least squares and constraint condition terms are minimized.

3. Results

In this section, the data from 748 GPS receivers that were available on the day of 23 March 2012 from the 0.25° × 0.25° grid (as shown in Figure 1) over the Japanese region were considered for the three-dimensional GPS tomography. Initially, to validate the algorithm, a 3-D electron density matrix of the required resolution was created from NeQuick model for that time, and then artificial GPS-TEC was deduced from the integrated electron density matrix along the actual GPS receiver locations to satellite paths for that time. Thus derived, the simulated TEC is given as input to the tomography algorithm to reconstruct the 3-D electron density.

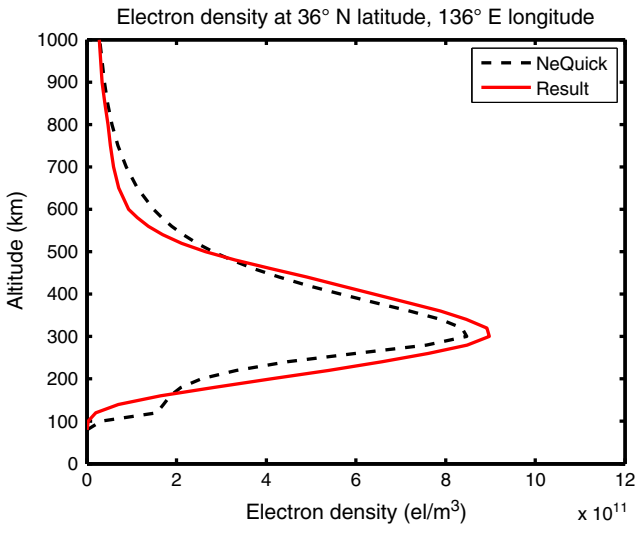

Figure 4. Electron density profile from (a) NeQuick model (black dashed line) and (b) simulated result (red line).

Figure 4 shows the comparison between the electron density profiles from the NeQuick model and the derived electron density from the simulated tomogram at the location 36°N latitude and 136°E longitude and at time 03:30 UT for 23 May 2012. It can be seen that simulated result electron density profile closely follows the model density profile as it is supposed to be. This simulation shows the ability of the algorithm to reconstruct the altitude density profile from the simulated GPS-TEC data without using the background ionospheric model as an initial guess.

And, the following Figures 5 and 6 show the comparisons between the model and the simulated reconstruction for both the vertical and spatial distributions

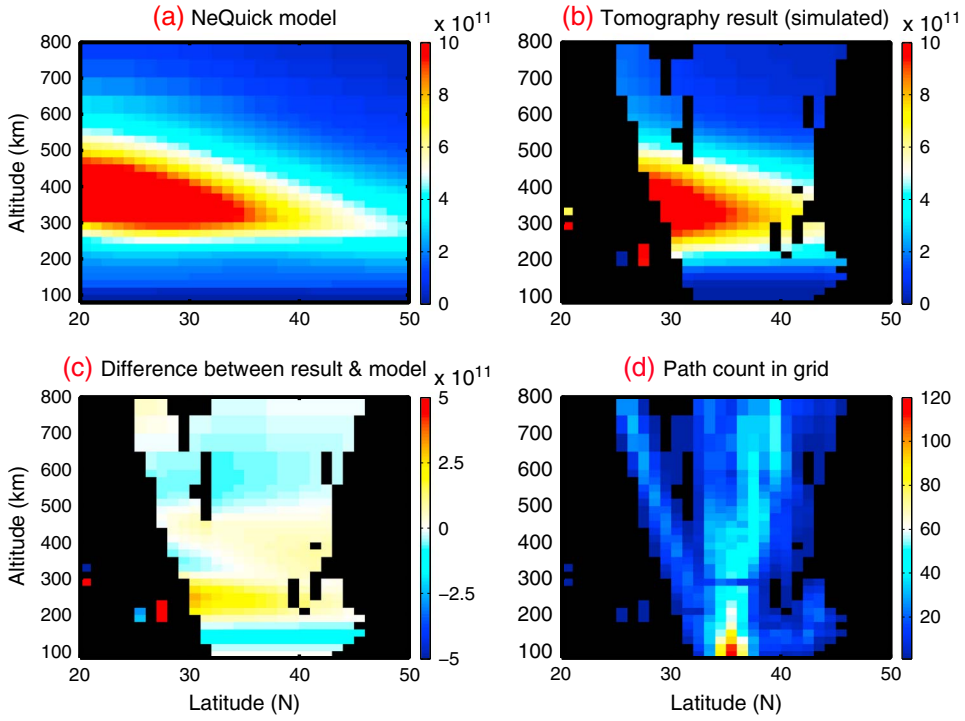

Figure 5. Two dimensional electron density structure (at 136° longitude) from (a) NeQuick model, (b) simulated result, (c) difference between model and simulation, and (d) path count in each grid/voxel.

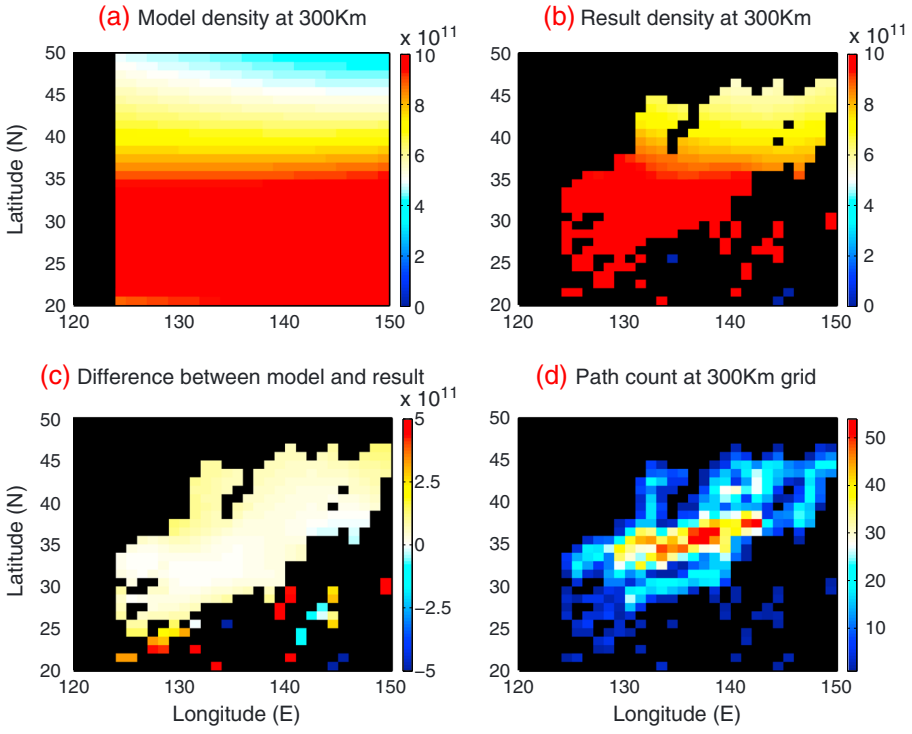

Figure 6. Horizontal structure of electron density (at 300 km altitude) from (a) NeQuick model, (b) simulated result (c) difference between model and simulation, and (d) path count in each grid/voxel.

of electron densities on 23 May 2012 at 03:30 UT. The two-dimensional latitude-altitude structure of electron density can be seen from NeQuick model output (Figure 5a), tomogram reconstruction using simulated GPS-TEC (Figure 5b), the associated error distribution (Figure 5c), and the GPS receiver-satellite path count in each grid box along the 136°E longitude plane (Figure 5d). And in Figures 5a and 5b, it can be seen that the simulated tomography results showed a similar distribution of the electron density compared to the NeQuick model density. In Figure 5c it can be seen that most of the differences in the electron density between the model and the simulated result are less than 1×10^{11} electrons/m^3, which is less than 10% of the maximum electron density in the profile. Figure 5d represents the number of data points or the path count (satellite-to-receiver line of sight intersections) present in each grid. This shows that the reliability in electron density reconstruction was not affected by the nonuniform data points in the grid other than where there the data points are down to zero. This can be attributed to the geometric limitation of the GPS observation paths and the minimum elevation angle that would limit the horizontal observations.

Figures 6a and 6b show the spatial electron density distribution at 300 km altitude derived from the model and the reconstruction from simulated result, respectively. It can be seen that the spatial reconstruction is also similar to the model-derived distribution, which can be inferred from the density differences between them that are less than 10% of the peak density as shown in Figure 6c. Figure 6d shows the path count; it is obvious that at this altitude of 300 km, there is enough path count or good coverage over Japan terrestrial. Also, the spatial reconstruction is seen relatively better than vertical reconstruction even in regions even where the path count falls moderately. Thus, from the different views of 3-D tomograms in Figures 4, 5, and 6, it can be inferred that the reconstruction of the 3-D electron density using simulated GPS-TEC is well reproduced and comparable to the model-derived 3-D density matrix, with some differences because of the inherent geometric limitation of the GPS data.

It is known that the data set lacks horizontal observations which are essential for tomography; hence, most tomography methods use a model for initial guess, and particularly, this technique does not use an initial guess to avoid biasing, but a constrained condition is used, described in the previous section. But the restrain parameter is derived from the model in this technique; therefore, to verify independency of model, a 100 km altitude shift in electron density profile was introduced by the model data. So the artificial GPS-TEC that was derived from NeQuick model electron density was altered by 100 km (by moving entire electron density altitude by 100 km) but without changing the restriction parameter C_{jk} to verify the robustness of the algorithm in reproducing the vertical profile. This simulated GPS-TEC was given as input to this tomography technique. As we can see that for the same day of 23 May 2012 and at 03:30 UT (Figures 7a and 7b), the tomography result also shifted up by around 60 to 70 km and shows similar distribution. In Figure 7a, the *F* region peak electron density altitude at 40°N is approximately 420 km, and the *F* region peak altitude obtained in the result (Figure 7b) is approximately 380 km at 40°N. But the peak electron density contours at around 30°N latitudes in both input (Figure 7a) and the result (Figure 7b) match reasonably good. And in Figure 7c, most of the density differences between the altitude-shifted model and the reconstruction are less than 15% of the peak density. The results show that the three-dimensional GPS ionospheric tomography algorithm performs reasonably okay in the reconstruction of the vertical and horizontal electron density distributions.

The rest of this section will use real-world GPS-TEC data obtained from the GEONET receiver locations shown in Figure 1, as the input for the 3-D tomography and for the same day on 23 May 2012. This would allow comparison in performance of the reconstruction of the algorithm using the actual GPS data against the simulated GPS-TEC and model density values. The actual GPS-TEC values when given as input instead of simulated values have also produced realistically good tomography images in both vertical and spatial distribution as shown in Figure 8 for the same time on 23 May 2012 at 03:30 UT.

The reconstruction of vertical structure of electron density from the GPS-TEC data can be seen in Figure 8a. Here the tomography reconstruction density still has similar and comparable features to the model (Figure 5a), but the difference between those density distributions is significant (about 20% of the peak density) as seen in Figure 8b and are larger when compared to differences between the model and simulation in Figure 5c. Figure 8c shows the spatial electron density distribution at 300 km altitude reconstructed from the GPS-TEC data. It can be seen that the spatial reconstruction features are similar to the model (Figure 6a), but the differences in magnitude are more than compared with simulation as seen in Figure 8d. From the path count in Figure 6d, it can be seen that these density differences grow more as the

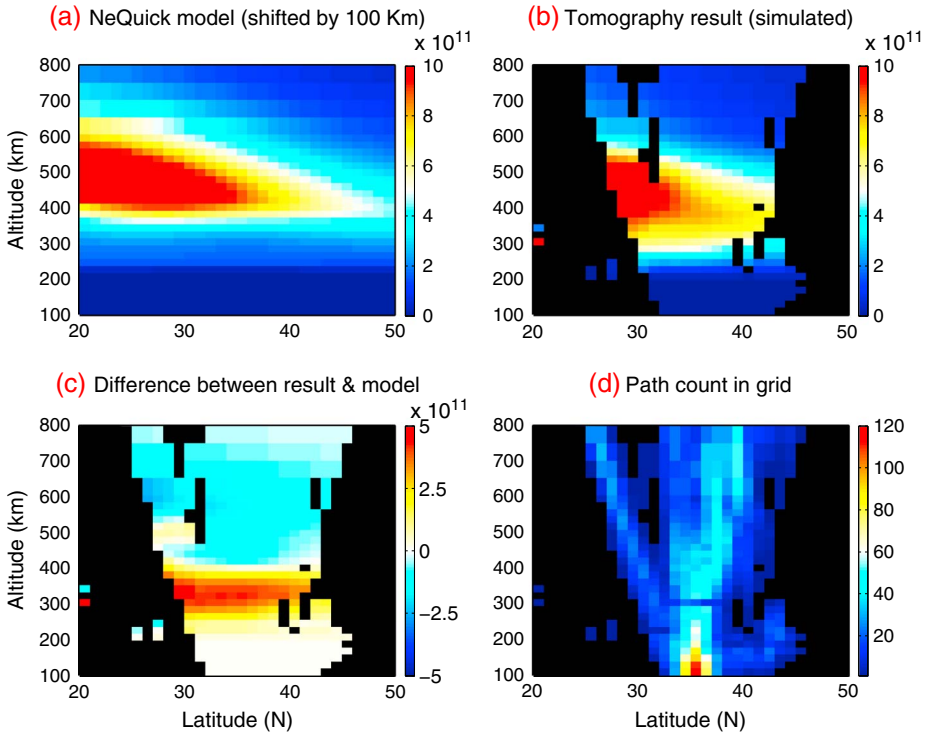

Figure 7. Vertical structure of electron density (at 136° longitude) from (a) NeQuick model shifted up by 100 km, (b) simulated GPS-TEC result, (c) difference between model and simulation, and (d) path count in each grid/voxel.

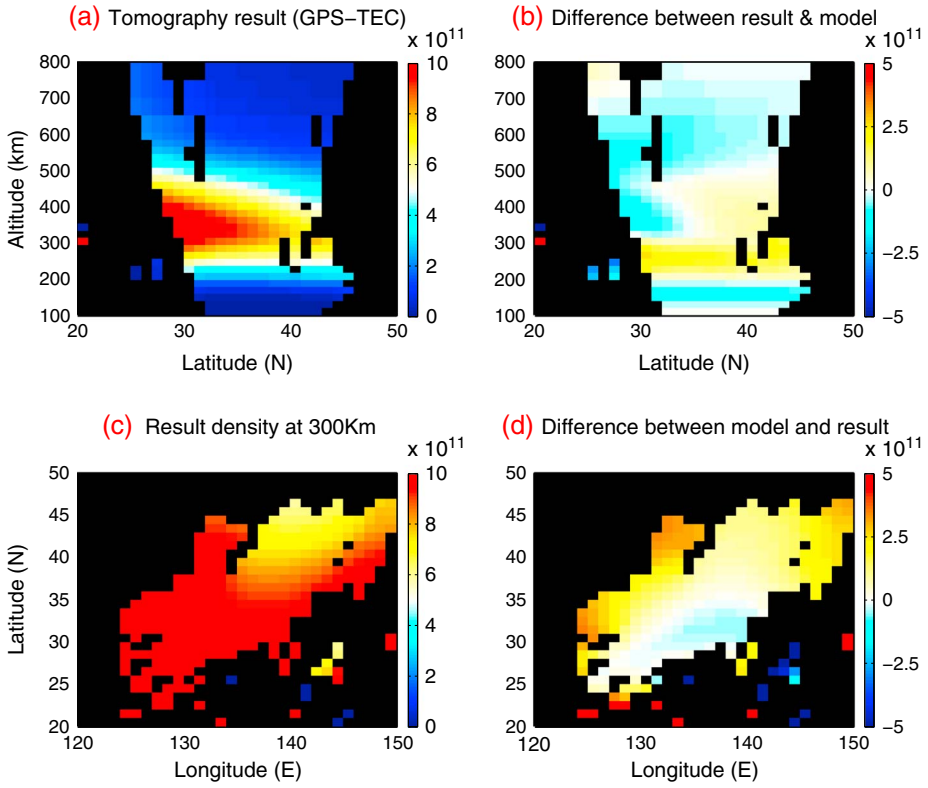

Figure 8. Tomography result from GPS-TEC (a) two-dimensional electron density structure at 136° longitude, (b) difference between model and result in vertical stratification, (c) spatial structure at 300 km, and (d) difference between model and result in spatial structure.

path count goes down. Also, a part in the reconstructed density difference compared to the model may be attributed to the fact that the empirical model will be different from the observed or measured densities.

4. Summary

This paper presents the newly developed three-dimensional GPS tomography of ionosphere using the TEC data from one of the densest GPS networks, GEONET in Japan. The technique primarily uses a constrained least squares fit without the requirement of initial guess from an ionospheric model. The technique uses a restrain parameter that constrains the altitude density profile with an assumption that the gradient of the election density is not large in the horizontal plane and can be large in the vicinity of the F_2 peak. And a hyperparameter balances the weight between the least squares and the constraint term while solving the cost function. Thus, the reconstructed electron density distributions are not biased by any empirical model.

The reconstructed tomography images are evaluated for reliability and flexibility in reproducing the electron density by using the simulated GPS-TEC data derived from NeQuick model and comparing with the electron density from NeQuick. This comparison between simulation and model shows that the tomography technique was successful in reconstruction of the three-dimensional electron density from the GPS-TEC data. And also in the real-world application, the reconstruction of electron density from the actual GPS-TEC data from GEONET also produced acceptable results.

With the spatial resolution set to 1° in latitude/longitude, the tomographic technique takes about 55 min to reconstruct the three-dimensional electron density images from the processed GPS-TEC data, on a high-end desktop PC. This calculation time is reduced to about 15 min when the horizontal resolution is decreased to 2° in latitude/longitude. Therefore, it is possible to implement a near real-time tomography maps over Japan for every 30 min or 1 h.

Acknowledgments

This work is supported by JSPS KAKENHI grant 22656092. Gopi K. Seemala was supported by "International Exchange Program" of National Institute of Information and Communications Technology (NICT). C.H. Chen is supported by the grant NSC102-2119-M006-007 from the National Science Council Taiwan and in part by the Headquarters of University Advancement at the National Cheng Kung University. We thank Pierdavide Coisson and Bruno Nava for their useful discussions about NeQuick model.

Robert Lysak thanks Yuichi Otsuka and an anonymous reviewer for their assistance in evaluating this paper.

References

Andreeva, E. S., V. E. Kunitsyn, and E. D. Tereshchenko (1992), Phase difference radiotomography of the ionosphere, *Ann. Geophys.*, *10*, 849–855.

Austen, J. R., S. J. Franke, C. H. Liu, and K. C. Yeh (1986), Applications of computerized tomography techniques to ionospheric research, paper presented at International Beacon Satellite Symposium June 9–14, Oulu, Finland, Proceedings Part 1, pp. 25–36.

Austen, J. R., S. J. Franke, and C. H. Liu (1988), Ionospheric imaging using computerized tomography, *Radio Sci.*, *23*(3), 299–307.

Chen, C. H. (2012), Modeling and observational studies of plasma density anomalies and earthquake-triggered disturbances in the mid-latitude ionosphere, PhD thesis, Dep. of Geophys., Kyoto Univ., Kyoto, Japan.

Fehmers, G. C., L. P. J. Kamp, F. W. Sluijter, and T. A. T. Spoelstra (1998), A model-independent algorithm for ionospheric tomography: 1. Theory and tests, *Radio Sci.*, *33*(1), 149–163, doi:10.1029/97RS03007.

Fremouw, E. J., J. A. Secan, and B. M. Howe (1992), Application of stochastic inverse theory to ionospheric tomography, *Radio Sci.*, *27*, 721–732.

Fridman, S. V., L. J. Nickisch, M. Aiello, and M. Hausman (2006), Real-time reconstruction of the three-dimensional ionosphere using data from a network of GPS receivers, *Radio Sci.*, *41*, RS5S12, doi:10.1029/2005RS003341.

Hansen, A. J., T. Walter, and P. Enge (1997), Ionospheric correction using tomography, paper presented at 10th International Technical Meeting, Proceedings of the Institute of Navigation GPS 97, Kansas City Convention Center, Kansas City, Mo.

Howe, B. M., K. Runciman, and J. A. Secan (1998), Tomography of ionosphere: Four-dimensional simulations, *Radio Sci.*, *33*(1), 109–128.

Iwabuchi, T., I. Naito, S. Miyazaki, and N. Mannoji (1997), Precipitable water vapor moved along a front observed by the Nationwide GPS Network of Geographical Survey Institute [in Japanese], *Tenki*, *44*, 3–4.

Kersley, L., J. A. T. Heaton, S. E. Pryse, and T. D. Raymund (1993), Experimental ionospheric tomography with ionosonde input and EISCAT verification, *Ann. Geophys.*, *11*, 1064–1074.

Ma, X. F., T. Maruyama, G. Ma, and T. Takeda (2005), Three-dimensional ionospheric tomography using observation data of GPS ground receivers and ionosonde by neural network, *J. Geophys. Res.*, *110*, A05308, doi:10.1029/2004JA010797.

Miyazaki, S., T. Saito, M. Sasaki, Y. Hatanaka, and Y. Iimura (1997), Expansion of GSI's nationwide GPS array, *Bull. Geogr. Surv. Inst.*, *43*, 23–34.

Otsuka, Y., T. Ogawa, A. Saito, T. Tsugawa, S. Fukao, and S. Miyazaki (2002), A new technique for mapping of total electron content using GPS network in Japan, *Earth Planets Space*, *54*, 57–62.

Radicella, S. M., and R. Leitinger (2001), The evolution of the DGR approach to model electron density profiles, *Adv. Space Res.*, *27*(1), 35–40.

Raymund, T. D. (1995), Comparisons of several ionospheric tomography algorithms, *Ann. Geophys.*, *13*, 1254–1262.

Raymund, T. D., J. R. Austen, S. J. Franke, C. H. Liu, J. A. Klobuchar, and J. Stalker (1990), Application of computerized tomography to the investigation of ionospheric structures, *Radio Sci.*, *25*, 771–789.

Raymund, T. D., Y. Bresler, D. N. Anderson, and R. E. Daniell (1994), Model-assisted ionospheric tomography: A new algorithm, *Radio Sci.*, *29*, 1493–1512.

Saito, A., S. Fukao, and S. Miyazaki (1998), High resolution mapping of TEC perturbations with the GSI GPS network over Japan, *Geophys. Res. Let.*, *25*, 3079–3082.

Saito, A., et al. (2001), Traveling ionospheric disturbances detected in the FRONT campaign, *Geophys. Res. Let.*, *28*, 689–692.

Tsuji, H., Y. Hatanaka, T. Sagiya, and M. Hashimoto (1995), Coseismic crustal deformation from the 1994 Hokkaido-Toho- Oki earthquake monitored by a nationwide continuous GPS array in Japan, *Geophys. Res. Let.*, *22*, 1969–1672.

Yeh, K. C., and T. D. Raymund (1991), Limitations of ionospheric imaging by tomography, *Radio Sci.*, *26*(6), 1361–1380, doi:10.1029/91RS01873.

Zhai, Y., and S. A. Cummer (2005), A flexible and robust direct reconstruction method for magnetospheric radio tomography, *Radio Sci.*, *40*, RS3004, doi:10.1029/2004RS003100.